Sustainable Cities and Society 99 (2023) 104914

Contents lists available at ScienceDirect

Sustainable Cities and Society

journal homepage: www.elsevier.com/locate/scs

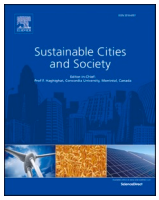

Data-driven analysis and integrated modeling of climate change impacts on coastal groundwater and sanitary sewer infrastructure

Yousef Sangsefidi [a,b,*], Austin Barnes [c], Mark Merrifield [c], Hassan Davani [b]

[a] Department of Mechanical and Aerospace Engineering, University of California–San Diego (UCSD), CA, USA
[b] Department of Civil, Construction, and Environmental Engineering, San Diego State University (SDSU), CA, USA
[c] Scripps Institution of Oceanography, University of California–San Diego (UCSD), CA, USA

ARTICLE INFO

Keywords:
Climate change adaptation
Sea-level rise
Coastal groundwater
Inflow and infiltration
Sanitary sewer infrastructure

ABSTRACT

The variation of the coastal groundwater table and the vulnerability of sanitary sewer infrastructure under a changing climate is considered for Imperial Beach (CA, USA) by incorporating the compound impacts of Sea-Level Rise (SLR), groundwater shoaling, and precipitation intensification. For 2 m of SLR, marine inundation is expected to impact only 2% of the urbanized area; however, SLR-driven groundwater shoaling is projected to impact 36% of the subterranean sewer system. Due to GroundWater Infiltration (GWI) and Rainfall-Derived Inflow and Infiltration (RDII), the sanitary sewage flow increases by 21% and 49% during dry- (i.e., consecutive days without precipitation) and wet-weather conditions (i.e., 24-hour rainfall with a 25-year return period), respectively. At SLR = 2 m, defect flows (GWI + RDII) can be elevated by 84% and 120% in dry- and wet-weather conditions, respectively. Such elevated hydraulic loads may place $0.5–$2.7 M additional cost on the collection system and treatment facilities every year. Moreover, pressurized junctions due to the above-mentioned hydraulic loading are likely to expose the community and the environment to raw sewage pollution. By involving structural, hydrological, and hydraulic criteria, a holistic approach is presented and implemented for prioritizing sewer system rehabilitation.

1. Introduction

An unequivocal sign of global climate change has been a 13.8 ± 1.5 cm rise in Global Mean Sea Level (GMSL) over the 20th century, which is more than that of the previous 27 centuries (Kopp et al., 2016). The rate of sea-level rise (SLR) has accelerated to 3.7 ± 0.5 mm/yr for the period 2006–2018 (Masson-Delmotte et al., 2021). Recent climate studies warn that depending on future greenhouse gas emissions, relative sea levels along the continental US coastline are projected to rise by ~0.6 − 2.2 m by the end of the century (Sweet et al., 2022). Besides the increasing exposure of ~1 billion people to overland flooding in coastal communities across the globe, SLR may also raise groundwater tables, posing a further threat to subterranean urban infrastructure systems and natural resources. Climate projections also raise concerns about how precipitation will respond in a warming world. While longer droughts are expected in most regions due to rising temperatures (attributed to higher surface evaporation), global models project a 16–24% increase in heavy precipitation intensity by 2100 (associated with the larger water-holding capacity of the warmer air) (Fischer et al., 2014; Trenberth, 2011). Thus, immediate attention is needed to understand the current and future interactions of oceanographic, hydrological, and meteorological processes (Fig. 1) and their possible stresses on coastal water resources and infrastructure systems (Befus et al., 2020; Bevacqua et al., 2019).

Over the current century, the projected SLR will threaten coastal infrastructure systems and ecosystems by shifting the coastline, accelerating beach erosion, and degrading coastal habitats (Arkema et al., 2013; Rotzoll & Fletcher, 2013). Currently, over 200 million people are exposed to marine flooding across the globe. Besides permanent marine inundation (Fig. 1), SLR also will escalate the frequency and magnitude of temporary elevated sea-level events (Thompson et al., 2021; Vitousek et al., 2017). A relatively small SLR of even 0.1 − 0.2 m may double the frequency of elevated sea-level events; therefore, a 1-m rise in GMSL could cause an increase of ~50% of the global population and assets at risk of marine flooding (Kirezci et al., 2020; Vitousek et al., 2017).

As shown in Fig. 1, coastal groundwater is dynamically connected to sea level. While the majority of previous studies on coastal aquifers [such as Watson et al. (2010); Lu et al. (2013); Mehdizadeh et al. (2014), and Badaruddin et al. (2015)] have focused on groundwater salinization

* Corresponding author.
E-mail address: ysangsefidi@ucsd.edu (Y. Sangsefidi).

https://doi.org/10.1016/j.scs.2023.104914
Received 6 March 2023; Received in revised form 30 July 2023; Accepted 1 September 2023
Available online 2 September 2023

Notations

A	Tidal efficiency
A_{eff}	Effective area of a conduit for groundwater infiltration (m^2)
C_d	Discharge coefficient of a circular orifice
CCTV	Closed-circuit television
D	Circular conduit diameter (m)
EGL	Energy Grade Level
EL_d	Rim elevation of the downstream node of a conduit (m)
EL_u	Rim elevation of the upstream node of a conduit (m)
GMSL	Global Mean Sea Level
GMW	Groundwater Monitoring Well
GWD	Groundwater Depth
GWI	GroundWater Infiltration (m^3/d)
GWT	GroundWater Table (m)
GWT_{ave}	Average GWT above a conduit (m)
g	Gravity acceleration ($\approx$ 9.81 m/s^2)
H_G	Groundwater head over a conduit (m)
HGL	Hydraulic Grade Line
h	Groundwater hydraulic head (m)
IB	City of Imperial Beach
K	Diagonal tensor of hydraulic conductivity (m/d)
L	Conduit length (m)
L_{eff}	Effective length of a conduit for groundwater infiltration (m)
LECZ	Low-Elevation Coastal Zone
MI	Marine Inundation
MSL	Mean Sea Level (m)
P	System porosity (%)
PCSWMM	Personal Computer Storm Water Management Model
POC	Point of connection between sewer systems
RDII	Rainfall-Derived Inflow and Infiltration (m^3/d)
SANDAG	San Diego Association of Governments
SFM	Sewer Flow Monitoring
SLR	Sea-Level Rise (m)
SSF	Sanitary Sewage Flow (m^3/d)
SSO	Sanitary Sewer Overflow
SSVI	Sanitary Sewer Vulnerability Index
T_{lag}	Tidal phase lag (hr)
W	Groundwater source and/or sink (d^{-1})
WWI	WasteWater Inflow (m^3/d)
ε	Soil void ratio

due to landward seawater intrusion, there is growing interest in studying groundwater flooding and its potential threats to infrastructure systems and coastal aquifers [e.g., Sangsefidi et al. (2023), Su et al. (2022), Teimoori et al. (2021), McKenzie et al. (2021), and Befus et al. (2020)]. Although flood control measures may protect Low-Elevation Coastal Zones (LECZ: areas with 0 – 10 m elevation above sea level) from marine flooding, coastal groundwater may respond to high sea-level events in the form of groundwater emergence and shoaling (Befus et al. 2020; Bevacqua et al. 2019). Numerical simulations of Su et al. (2022) for the city of Hoboken (New Jersey, USA) indicated that groundwater starts to emerge for SLR = 0.4 m, and one-third of the city will experience subsurface flooding for a 1-meter SLR scenario. The increased risk of groundwater inundation has been confirmed for other areas such as Miami, Honolulu, San Francisco Bay Area, and Philadelphia (Cooper et al. 2015; Habel et al. 2017; Plane et al. 2019; Rossi and Toran 2019).

In metropolitan areas, the existence of shallow groundwater (having a depth of 0 – 2 m) can cause serious problems in the operation and maintenance of subterranean infrastructure systems (Habel et al. 2020; Rotzoll and Fletcher 2013). As shown in Fig. 1, a high-level groundwater table may reduce the discharge capacity of urban drainage networks through groundwater infiltration (GWI) into network defects, holes, and cracks (Dirckx et al. 2016; Liu et al. 2018). GWI may constitute up to one-third of sanitary sewage flow, which can triple in LECZs with a 1-m SLR (Fung and Babcock 2020; Zhao et al. 2020). It is worth noting that compared to pipe geometries and surrounding soil characteristics, the parameter with the greatest effect on GWI is the groundwater table elevation (i.e., groundwater head over pipes) (Liu et al. 2021). In addition, Rainfall-Derived Inflow and Infiltration (RDII) may cause a further reduction in the available hydraulic capacity of defective sanitary sewer systems during wet-weather conditions (Rezaee and Tabesh 2022).

The enhanced awareness of compound event impacts has recently

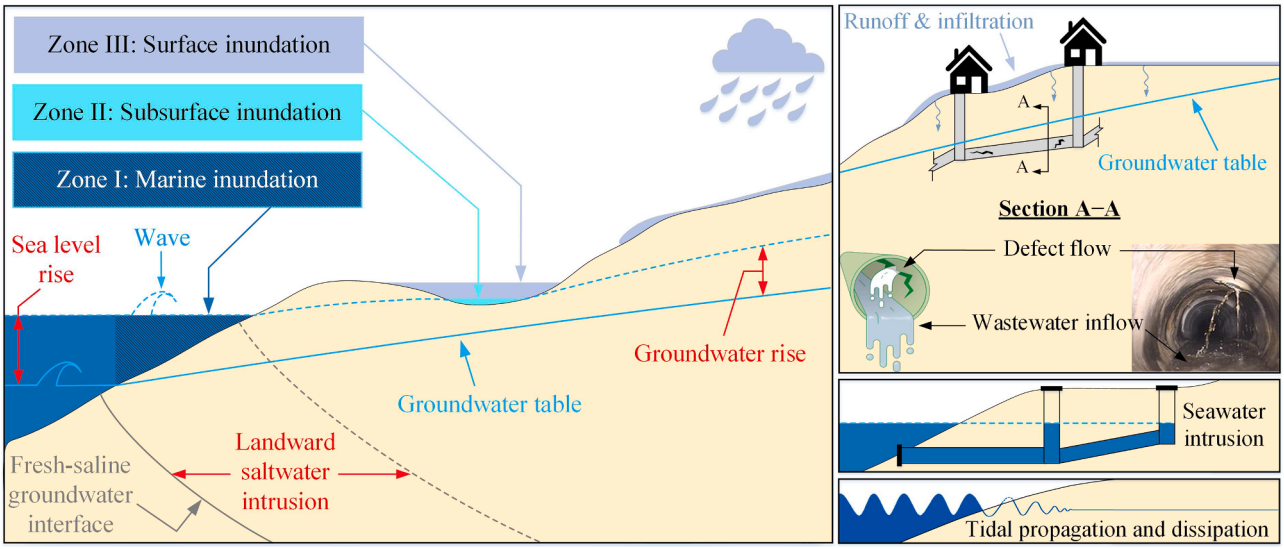

Fig. 1. Schematic view of different coastal stressors along with current (solid line) and future (dashed line) conditions of sea level, groundwater table, and fresh-saline groundwater interface.

motivated researchers to assess the vulnerability of storm drain infrastructure systems against compound sources of flooding from seawater, groundwater, and stormwater flows (Gold et al. 2022; Laster Grip et al. 2021; Sangsefidi et al. 2023). To establish efficient adaptation strategies, however, there is an urgent need for an improved understanding of the coastal stressors on sanitary sewer systems and new assessments of their interactions. Thus, the principal objectives of this study are to provide new insights into the interactions of coastal groundwater with surface-water bodies and to identify the exposure of sanitary sewer systems to subsurface flooding in a changing climate. To achieve these goals, we focus on Imperial Beach (IB) in Southern California as an urban laboratory, for which a 3D and high-resolution groundwater model has been developed using Visual MODFLOW Flex version 8.0 and incorporating site-specific conditions. Due to the lack of groundwater data in this community near the US-Mexico border, we installed four monitoring wells inside IB, and groundwater table measurements were utilized for calibrating the groundwater model. In addition, the performance of IB's sanitary sewer system is simulated using the Personal Computer Storm Water Management Model (PCSWMM, version 7.5.3406). ArcGIS is also used for geospatial analysis and flood mapping.

2. Material and methods

2.1. Study area

This study focuses on a case study of Imperial Beach (IB) as the southwestern-most city in the continental United States with ~30k population (mostly Hispanic or Latino demographics according to 2019 census estimates), ~2.5 km coastline, ~5.5 km^2 area, and 2 – 10 m elevation (Gallien 2016). As shown in Fig. 2, IB's residential area is surrounded by the Pacific Ocean, San Diego Bay, and the Tijuana Estuary on three sides, and therefore, IB has historically experienced surface-water flooding. Due to its unique setting, this low-lying coastal community is also vulnerable to subsurface flooding during high sea-level conditions. Additional coastal stressors may impact aging water infrastructure systems in this underserved community in Southern California, especially due to SLR.

Fig. 3 illustrates the domains of groundwater and sewer system models developed for the study area. For observing unconfined aquifer levels (required for the groundwater model calibration), we drilled and installed four groundwater monitoring wells in December 2021 around IB's frequently flooded areas (GMW 1–4 in Fig. 3). As presented in Fig. 4 and Table 1, the sewage flow is collected across three tributary areas (sewer zones *I*–III with slight upward slopes from the surrounding water bodies) through ~66 km gravity and ~8 km force mains (ranging 0.102–0.610 m in diameter) connected to 11 pump stations. The flow is eventually discharged into the City of San Diego sewer system through three connection points (POC 1–3). While the useful life of Vitrified Clay (VC) pipes is roughly 50–60 years, about 84% of IB's sewer length consists of VC pipes, of which more than 90% were installed before the 1970s (Table 2). A closed-circuit television (CCTV) sewer inspection in 2014–2015 confirms that about one-third of sewer lines currently have a significant degree of structural damage (visualized in Fig. 5), and this ratio is expected to increase as the system ages over the century with lack of proper system maintenance in an underserved community. Defective sewer elements are susceptible to increased hydraulic load due to GWI and/or RDII.

The research team has established a working relationship with the City of IB, whose managers and decision-makers have expressed strong interest in using the results of this research to promote public safety against SLR and other climate change consequences. It should be noted that although the focus of this research is on IB, the modeling approach is generalizable to other coastal communities after considering their site-specific conditions.

2.2. Primary datasets

Table 3 presents the main datasets utilized in the present study. A Digital Elevation Model (DEM with 0.762 $m \times 0.762$ m resolution) and a parcel layer are acquired from the data warehouse of the San Diego Association of Governments (SANDAG). The sea-level records in San Diego Bay (station ID: 9,410,170) are obtained from the National Oceanic and Atmospheric Administration (NOAA). Following NOAA's regional SLR scenarios (Sweet et al. 2022), we examine SLR = 0, 1, 2,

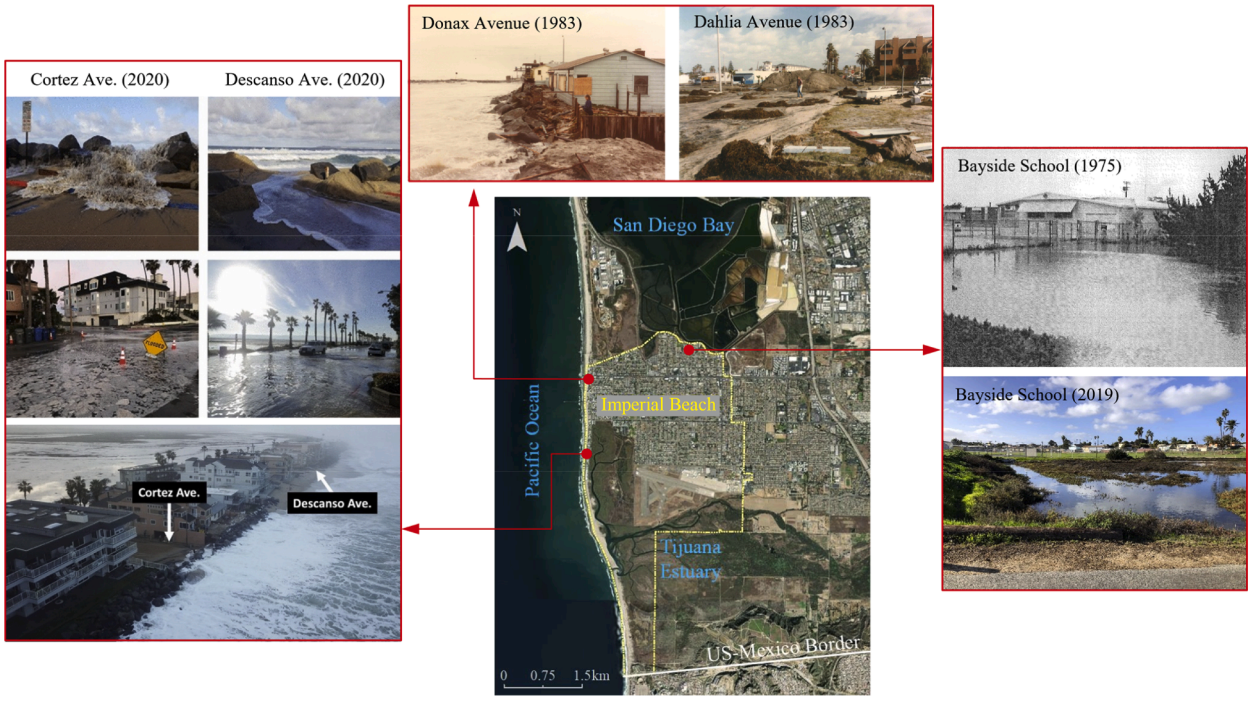

Fig. 2. Examples of marine-based flooding in Imperial Beach: (left) ocean wave overtopping (Merrifield et al. 2021); (right) Bayside School flooding by high tides (courtesy of the City of IB); (top) debris cleanup efforts after a storm in 1983 (courtesy of the City of IB).

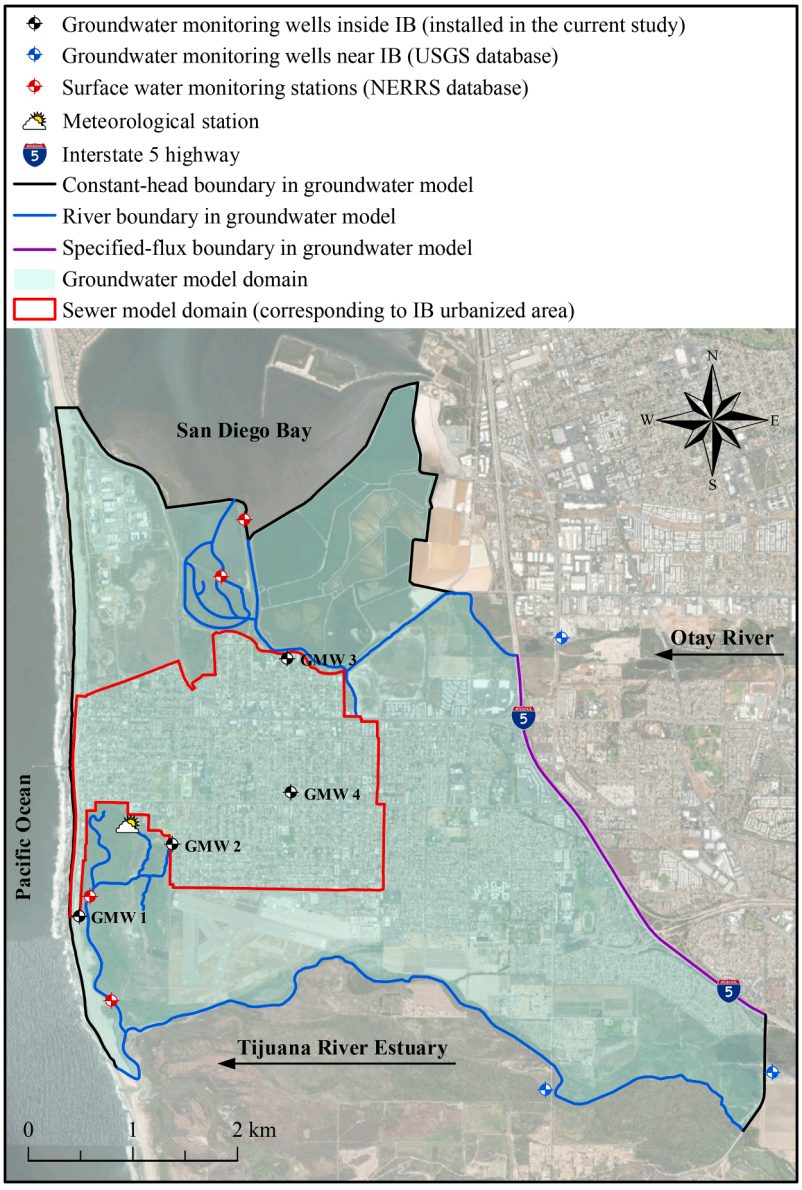

Fig. 3. Domains of the groundwater and sewer models.

and 3 m. While SLR = 0 m refers to the present-day Mean Sea Level [MSL = 0.811 m at IB referenced to the North American Vertical Datum of 1988 (NAVD88)], the studied scenarios of SLR = 1, 2, and 3 m are associated with intermediate, high, and extreme greenhouse-gas emission scenarios over the century (Sweet et al. 2022). For developing the groundwater model using Visual MODFLOW Flex, monitoring data on river levels and groundwater tables around IB are acquired from nearby sites from the United States Geological Survey (USGS) and the National Estuarine Research Reserve System (NERRS) websites (station locations are depicted in Fig. 3). The IB monitoring wells we installed are described in Section 2.3.2.

The main input parameters for the sanitary sewer model (PCSWMM described below in 7 section ws preroiesprre oepree aesee era -eos wssso wawssi wpsspepsesprrwe era)4.3.2 irrpsroprn wssens e rs. ros nsrmetric and spatial specifications of the sewer system elements (e.g., junctions, conduits, and pump stations) are obtained from the City of IB by request, whose gaps are filled through the field and virtual visits performed by our team. Defective conduits are identified and classified based on CCTV sewer inspections conducted in IB during December 2014 – January 2015 (courtesy of the City of IB). A GIS parcel layer –available in the SANDAG data warehouse– is utilized for the estimation of wastewater loads from each land-use unit. Utilizing NOAA's precipitation-frequency data, a 24-hour rainfall with a 25-year return period is selected to represent a reasonably significant storm condition that is likely to occur within the next couple of decades. Other parameters involved in the calibration of the groundwater and sewer models (e.g., hydraulic conductivity, groundwater recharge, conduit roughness, and monitoring data on rainfall and sewage flow) are obtained or set by referring to local sources (described in Sections 2.3.3 and 2.3.4).

2.3. Methods

Fig. 6 presents the workflow carried out in the present study. The methodologies used to conduct the mentioned tasks are described in the following subsections.

2.3.1. Groundwater monitoring

The four groundwater monitoring wells were drilled using an 0.203-m hollow stem auger down to a depth of 6.096 m or 20 ft (drill cuttings were collected every 1.524-m for soil analysis). The well casing is 0.051

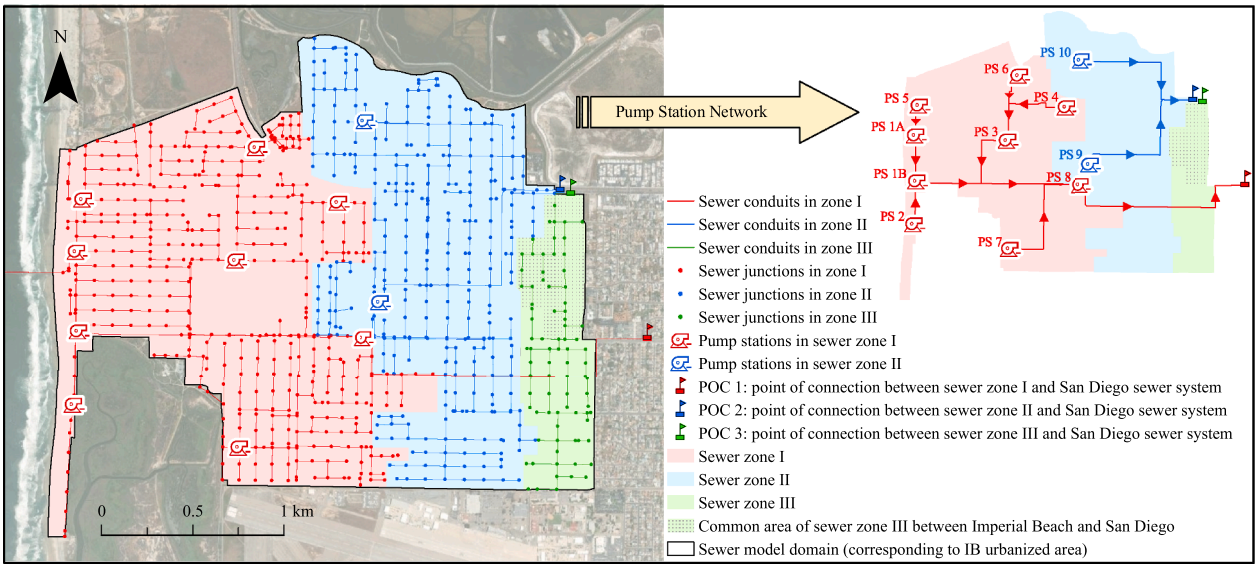

Fig. 4. Specifications of the sanitary sewer model.

Table 1
Sewer lengths (in percentage) with different sizes (total length = 74,289 m).

Diameter (m)	Gravity mains	Force mains	Total
0.102	0.2%	0.0%	0.2%
0.152	19.1%	0.4%	19.5%
0.203	61.0%	0.5%	61.5%
0.254	3.5%	2.4%	5.9%
0.305	3.0%	7.2%	10.3%
0.381	1.4%	0.0%	1.4%
0.406	0.1%	0.0%	0.1%
0.457	0.1%	0.3%	0.5%
0.533	0.4%	0.0%	0.4%
0.610	0.1%	0.0%	0.0%
Total	89.2%	10.8%	100.0%

Table 2
Sewer lengths (in percentage) with different material constructed in each decade (total length = 74,289 m).

Decade Constructed	Sewer material [I]				Total
	VC	PVC	CI	DI	
1940s	10.7%	0.0%	0.1%	0.0%	10.8%
1950s	55.8%	2.5%	1.0%	0.0%	59.3%
1960s	10.2%	0.4%	0.0%	0.0%	10.6%
1970s	7.0%	1.7%	0.0%	0.0%	8.7%
1990s	0.0%	3.8%	0.0%	0.0%	3.9%
2000s	0.5%	4.6%	0.0%	0.1%	5.1%
2010s	0.1%	1.5%	0.0%	0.0%	1.6%
Total	84.3%	14.6%	1.1%	0.1%	100.0%

[I] VC, PVC, CI, and DI respectively refer to vitrified clay, polyvinyl chloride, cast iron, and ductile iron.

m in diameter, and the bottom 3.048 m of each well is screened with 0.0005 m perforations. The wells were permitted and finished according to San Diego County regulations: the bottom 3.658 m was filled with #3 filter pack sand, above that 1.524 m of the annular seal bentonite, and finally 0.914 m of surface concrete to seal the well.

Each well was equipped with a 0.0254 m diameter RBR Solo pressure sensor with sampling at 1 Hz frequency, suspended between 0.914−1.828 m above the well bottom. Atmospheric pressure measurements taken every 6 min at NOAA meteorological station 9,410,170 in San Diego Bay were interpolated to 1 second and then subtracted from the RBR pressure measurements. The remaining pressure is assumed to be hydrostatic pressure. The salinity structure of each well was determined using a conductivity-temperature-depth survey every two months, which was relatively fixed over the observation period. Thus, the average densities were used to convert hydrostatic pressure to groundwater depth. Reference depths (from the well heads to the water tables) and wellhead elevations were measured using a Solinst water-level meter and GPS, respectively.

The continuous records from December 8, 2021 to June 5, 2022 are analyzed to determine the time-averaged groundwater table (GWT) and tidal influence in each well. The latter is described by two parameters of phase lag (T_{lag} = time delays between sea level and GWT signals) and tidal efficiency (A = ratio of amplitude variation in a well compared to ocean-tide amplitude) (Su et al. 2022). The pure tidal signal for each GMW (determined by the Python package UTide) is cross-correlated with the pure tidal signal from the tide gage using the Python package SciPy. Then, the tidal phase lag with the highest correlation is selected as the lag time between the ocean and the GWT. Linear regressions on the pure tidal signals of GMWs versus the tide gage are performed, and the slopes of the linear regressions are reported as the tidal efficiency (A) at each GMW.

2.3.2. Groundwater modeling

Incorporating site-specific conditions, a three-dimensional and steady-state groundwater flow model is developed for the coastal unconfined aquifer using the open-source MODFLOW-2005 engine (distributed by USGS) implemented in the graphical interface of Visual MODFLOW Flex [developed by Waterloo Hydrogeologic (2021)]. Based on a finite difference numerical scheme (Domínguez-Vázquez, Jacobs, & Tartakovsky, 2021), MODFLOW has been widely used for groundwater flow modeling by previous researchers such as Su et al. (2022) and Befus et al. (2020).

The equilibrium water-table responses to sea-level rise can be described by the following partial differential equation, which is a combination of Darcy's Law with the conservation of mass:

$$\nabla.(K\nabla h) = W \quad (1)$$

where h = groundwater hydraulic head; $\boldsymbol{K}$ = diagonal tensor of hydraulic conductivity; and W = volumetric flux per unit volume representing sources and sinks (Harbaugh 2005). Fig. 3 illustrates the groundwater model domain and its side boundary conditions. While the domain is extended to major surface-water bodies and groundwater divides, it is discretized into ~1 million cells in a one-layer model with a

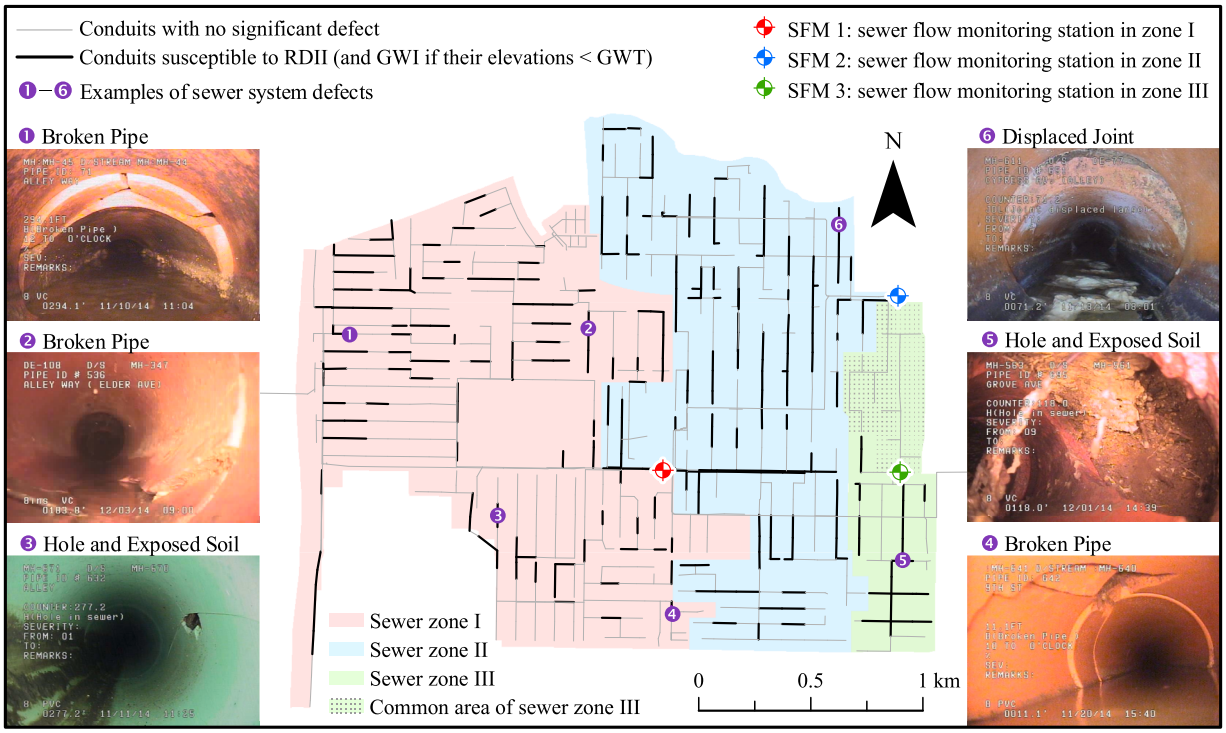

Fig. 5. Defective conduits and sewer flow monitoring stations.

Table 3
Main datasets used in the present study.

Data		Source	Description
Digital Elevation Model		SANDAG ArcGIS Server	Resolution: 0.762 $m\times$ 0.762 m
Land-use parcel layer			Used for the estimation of wastewater production across the city
Surface-water level	MSL & SLR scenarios	NOAA–Tides and Currents	MSL = 0.811, 1.811, 2.811, and 3.811 m for SLR = 0, 1, 2, and 3 m
	River level	NERRS	Referring to TJRBRWQ, TJROSWQ, TJRPRWQ, TJRSBWQ stations
Groundwater table	Inside IB	N/A	Installing four groundwater monitoring wells in IB in the current study
	Near IB	USGS–National Water Information System	No active groundwater site inside IB
Sanitary sewer system	Geometric & spatial data	City of Imperial Beach	Available at the data warehouse of the City of IB
	CCTV inspection		Conducted in Dec. 2014 – Jan. 2015 by Tran Consulting Engineers
	Monitoring sewage flow		Conducted in Dec. 2016 by V&A Consulting Engineers
Rainfall data	Monitoring rainfall data	NERRS	TJRTLMET station records over the period of sewage flow monitoring
	24-hour storm	NOAA Atlas	Referring to 24-hour NOAA precipitation-frequency data

high resolution of 7 m × 7 m to represent topography details. The model bottom was set to the elevation -50 m NAVD88 (covering the quaternary deposits placed above the San Diego formations with a low hydraulic conductivity) with a no-flow boundary condition (assuming a horizontal groundwater flow at the bottom) (Befus et al. 2020; Stuart 2008). A drain–recharge boundary condition is applied to the model top to serve as either a groundwater discharge or recharge feature for levels at or below the ground surface, respectively. Considering a high and low conductance drain for natural and urbanized areas (5 – 500 m^2/d), the spatial recharge rates are prescribed by the annual effective recharge (4 – 12 mm/yr), from which evapotranspiration fluxes are already removed (Reitz et al. 2017). According to the sensitivity analysis conducted by Sangsefidi et al. (2023) on the study area, $\boldsymbol{K} = 1$ m/d is set in the model by assuming a homogeneous and isotropic aquifer. For the model calibration, the modeled GWT at MSL is compared with the temporal mean values of the observed GWT from the installed wells (section 3.1).

2.3.3. Flood mapping

The locations impacted by marine inundation (MI) are determined using a bathtub approach, in which the sea-level elevation in a given SLR scenario is subtracted from the DEM raster data to identify the areas with elevations lower than MSL (Habel et al. 2020). The identified locations without a surficial connection to the seawater source are excluded from MI. However, these areas are still threatened by subsurface flooding (Rotzoll and Fletcher 2013). By subtracting GroundWater Table (GWT) values from the DEM, a similar method is applied to identify the areas potentially vulnerable to groundwater emergence and shoaling. In addition, considering the small variations of GWT over conduits (< 3 cm changes in GWT for 98% of conduits), its average value above each conduit (GWT_{ave}) was determined by ArcGIS and utilized for estimation of groundwater head (H_G) over subsurface sewer infrastructure.

2.3.4. Sewer system modeling

The performance of the sewer system is evaluated by developing and calibrating a PCSWMM model that is supplemented by flow monitoring data and CCTV inspection data. Using the SWMM version 5.1 engine, this model is widely used for simulating wastewater, stormwater, and combined infrastructure systems (Sangsefidi et al. 2023; Tavakol-Davani et al. 2016). Recalling from Fig. 4, the separate sewer system is modeled in a substantially high resolution by having 920 conduits

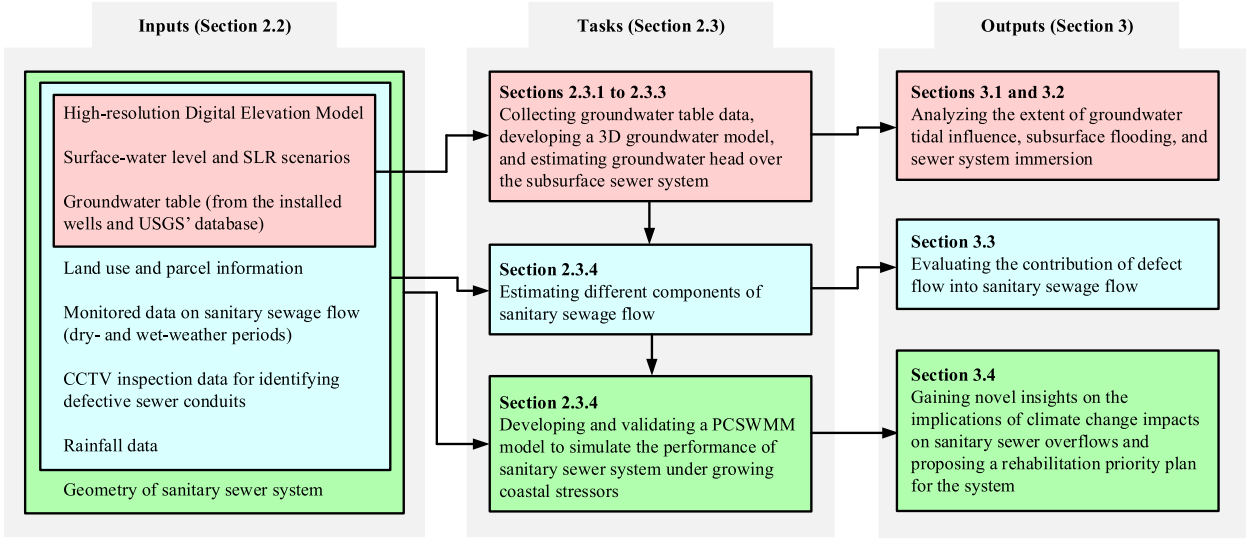

Fig. 6. Schematic diagram of the present study workflow.

distributed across the three sewer zones. Using a combination of gravity and pumping systems, sewage flows from sewer zones I and II to POC 1 and 2, respectively. However, only a gravity system transfers the flow from zone III to POC 3. At the three locations shown in Fig. 5, flow monitors were installed by the City of IB in sewer manholes for two weeks beginning on December 15th, 2016. As essential data sources for calibrating the PCSWMM model, the flow monitors were able to measure the sewage flow leaving the three sewer zones in both dry and wet weather conditions (Fig. 7).

According to Eq. (2) and Fig. 1, the sanitary sewage flow (SSF) consists of WasteWater Inflow (WWI) and defect flow (= GWI + RDII) (Rezaee & Tabesh 2022). These components of SSF are described in the three following sections.

$$\text{SSF} = \text{WWI} + \text{Defect Flow}$$
$$\text{Defect Flow} = \begin{cases} 0 & \text{for a non-defective system} \\ \text{GWI} & \text{for a defective system in dry weather} \\ \text{GWI} + \text{RDII} & \text{for a defective system in wet weather} \end{cases} \quad (2)$$

2.3.4.1. WWI estimation. To estimate WWI and assign its corresponding loads to the city-wide sewer system, a multi-step GIS analysis is conducted. The land-use parcel map (Fig. 8) is created by applying the GIS 'Spatial Join' tool on available geospatial layers of land-use zones and urban parcels. Daily average WWI rates are determined for different land-use categories according to the Sewer Design Guide of The City of San Diego (2015) (Table 4). Then, individual WWI loads from each urban parcel (Fig. 8) are attributed to their nearby sewer junctions using the GIS 'Near' tool and subsequently imported into PCSWMM as junction baselines. According to the diurnal pattern presented in Fig. 7, WWI loads during peak hours are also estimated by multiplying daily average WWI loads by a factor of 1.4.

2.3.4.2. GWI estimation. The defect flow primarily includes GWI and RDII. In the case of having a defective system located under the GWT, groundwater constantly infiltrates into the system through its immersed defects. This study considers GWT elevation and system porosity (P = ratio of defect-to-conduit surface area) as the two main parameters affecting GWI. According to Eq. (2), GWI values for the three sewer zones are estimated by subtracting their daily-averaged dry-weather SSF (Fig. 7) from the estimated WWI (presented in Table 5 and previously described in this section). Then, by assuming that system defects are in an idealized circular form and uniformly distributed on defective conduits, the parameter P is adjusted in each of the three sewer zones such that the calculated GWI from Eq. (3) matches the estimated value from the monitoring data (during dry-weather conditions: GWI = SSF - WWI). This equation is a modified form of the head-discharge equation for a circular orifice, which assumes that the surrounding soil is homogeneous and isotropic, and not significantly washed out into the pipes (Guo and Zhu 2017). In this equation, ε = void ratio of the surrounding soil [= 0.2 according to the Web Soil Survey of The United States Department of Agriculture (2019)]; C_d = discharge coefficient of a circular orifice [= 0.6 according to Swamee and Swamee (2010)]; g = gravity acceleration; H_G = groundwater head over conduits; and A_{eff} = effective conduit area receiving GWI (Fig. 9). It is worth noting that by assuming insignificant changes happening in the sewer system deficiency over the time, the calibrated P values for the existing system are considered for future scenarios too (ranging from 0.0015 to 0.0027). However, GWI variations with SLR are considered by involving A_{eff} and H_G parameters (which can be estimated based on the modeled GWT by MODFLOW). The calculated GWI for each defective and immersed conduit is allocated to its upstream junction as an additional baseline in the PCSWMM model.

$$\text{GWI} = \frac{PA_{eff}}{2160000\pi}\varepsilon C_d\sqrt{gH_G} \quad (3)$$

2.3.4.3. RDII estimation. Unlike GWI, RDII only occurs during rainfall events, and it can be obtained by subtracting dry-weather SSF from wet-weather SSF. As shown in Fig. 7, the rainfall event during the sewer flow monitoring period occurred on December 21−22, 2016 with a total depth of 40.9 mm (determined based on the area under the rainfall hyetograph). As presented in Table 5, the resulting RDII from this rainfall event is estimated as the difference between SSF values from the wet- and dry-weather monitoring periods. For the estimation of RDII from a different rainfall event, it is assumed that the total depth of a rainfall event and its resulting RDII are proportional. For example, the total depth of a rainfall event with a 25-year return period is 69.6 mm, which is 70% larger than that of the monitored storm (69.6 ÷ 40.9 = 1.70). Thus, the monitored RDII values for each sewer zone (reported in Table 5) are multiplied by 1.7 to estimate the RDII for a 25-year storm. The resulting RDII values are assigned to upstream junctions of defective conduits as a wet-weather baseline in PCSWMM. To account for projected increases in precipitation associated with climate change, we assume a 25% increase in heavy precipitation intensity for southern California by 2100 based on Fischer et al. (2014). A similar method is

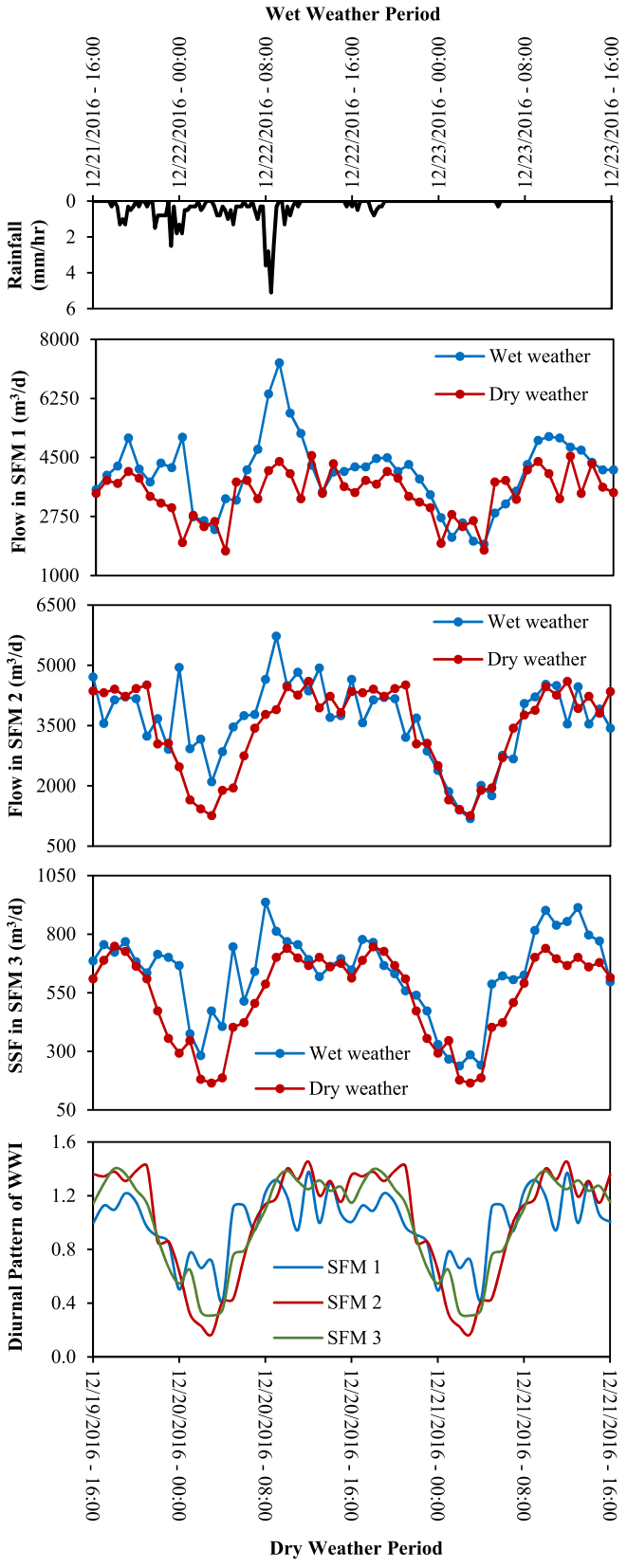

Fig. 7. Monitored Sanitary Sewage Flow (SSF) during dry- and wet-weather periods.

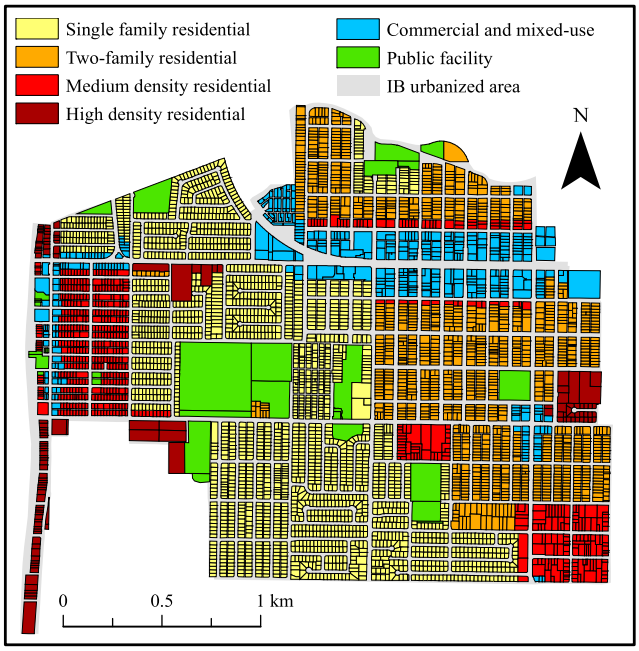

Fig. 8. Land-use parcels in IB.

Table 4
Wastewater inflow rates for different land uses.

Land-use category	WWI rate (m^3/d)
Single family residential	0.570 (per parcel)
Two-family residential	0.494 (per 280 m^2 or 1 DU)
Medium density residential	0.456 (per 185 m^2 or 1 DU)
High density residential	0.418 (per 140 m^2 or 1 DU)
Commercial and mixed-use	7.733 (per 4047 m^2 or 1 acre)
Public Facility	9.503 (per 4047 m^2 or 1 acre)

applied to consider potential additional RDII loads from the precipitation intensification for scenarios corresponding to SLR = 1–3 m.

After assigning three components of SSF to corresponding junctions in PCSWMM, flow routing within conduits is simulated by solving the conservation of mass and momentum (i.e., 1D Saint-Venant equations) using the Finite Difference Method (Rossman 2015; Domínguez-Vázquez, Klose, & Jacobs, 2023). While Hazen-Williams coefficients of 150, 120, and 90 are respectively assigned to PVC, DI, and CI sewer force mains, Manning's roughness coefficients for VC and PVC gravity mains are considered 0.014 and 0.011 [Engineering ToolBox (2004a) and (2004b)]. In addition, entry and exit loss coefficients of conduits range from 0.1 − 0.6 based on their relative sizes (Frost 2006). To evaluate the effects of SLR, system porosity, and rainfall properties on the performance of sanitary sewer systems, 17 scenarios are defined as presented in Table 6.

3. Results and discussion

3.1. Groundwater table variations in monitoring wells

Fig. 10 presents the time series of groundwater depth and head for the four monitoring wells across IB. From Fig. 10(a), the GWT near the coast is the shallowest and most heavily influenced by ocean tides (GMW 1 shown in Fig. 3). However, the observed GWT in other wells (GMW 2 − 4) are deeper, farther from the nearest coastline, and nearly stationary in comparison to GMW 1. Having semi-diurnal tidal fluctuations (i.e., two low and two high tides per day), the average GWT is approximately 0.2 − 0.4 m above MSL [Fig. 10(b)]. Except for GMW 1 located in the small peninsula between the Pacific Ocean and the Tijuana Estuary,

Table 5
Comparison of daily-averaged values of monitored and modeled sanitary sewage flows.

Station	Monitored SSF (m^3/d)			Modeled SSF (m^3/d)			Difference (%)
	Dry weather (WWI + GWI)	Wet weather (WWI + GWI + RDII)	RDII (wet weather – dry weather)	WWI	Dry weather	Wet weather	Dry/Wet weather
SFM 1	3448.1	4027.7	579.5	2953.0	3447.2	4027.1	0.0%
SFM 2	3427.7	3773.3	345.6	2603.2	3427.7	3772.6	
SFM 3	534.1	625.4	91.2	523.3	534.1	625.3	
Total	7410.0	8426.3	1016.4	6079.5	7409.0	8425.0	

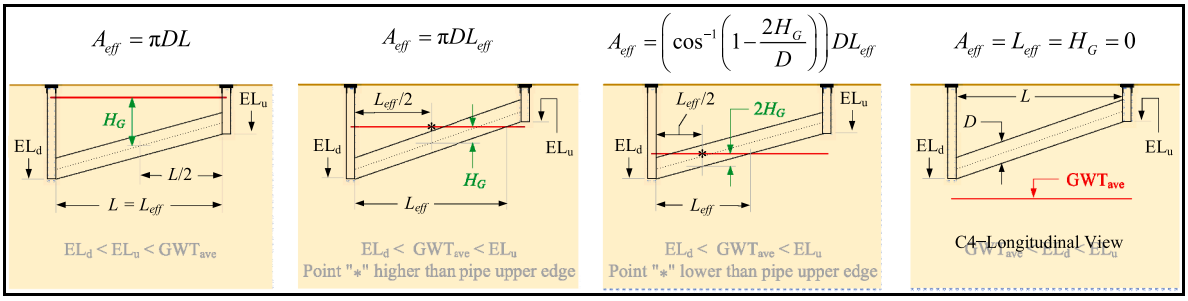

Fig. 9. Different situations of conduits with respect to GWT_{ave}.

Table 6
Studied scenarios in the present study.

Sanitary sewer system	Wastewater	Weather [I]	SLR (m)			
			0	1	2	3
Defective	Daily mean	Dry	WWm_SLR0_Dry	WWm_SLR1_Dry	WWm_SLR2_Dry	WWm_SLR3_Dry
		Wet [II]	WWm_SLR0_Wet	WWm_SLR1_Wet	WWm_SLR2_Wet	WWm_SLR3_Wet
	Daily peak [III]	Dry	WWp_SLR0_Dry	WWp_SLR1_Dry	WWp_SLR2_Dry	WWp_SLR3_Dry
		Wet	WWp_SLR0_Wet	WWp_SLR1_Wet	WWp_SLR2_Wet	WWp_SLR3_Wet
Non-defective	Daily mean	Dry/Wet	WWm			

[I] Wet weather condition refers to a 24-hour rainfall with a 25-year return period.
[II] To consider climate change effects on precipitation intensity, a 25% increase in RDII is applied for the scenarios corresponding to SLR = 1–3 m.
[III] Daily peak wastewater is approximately 40% larger than the daily mean value (diurnal pattern presented in Fig. 7).

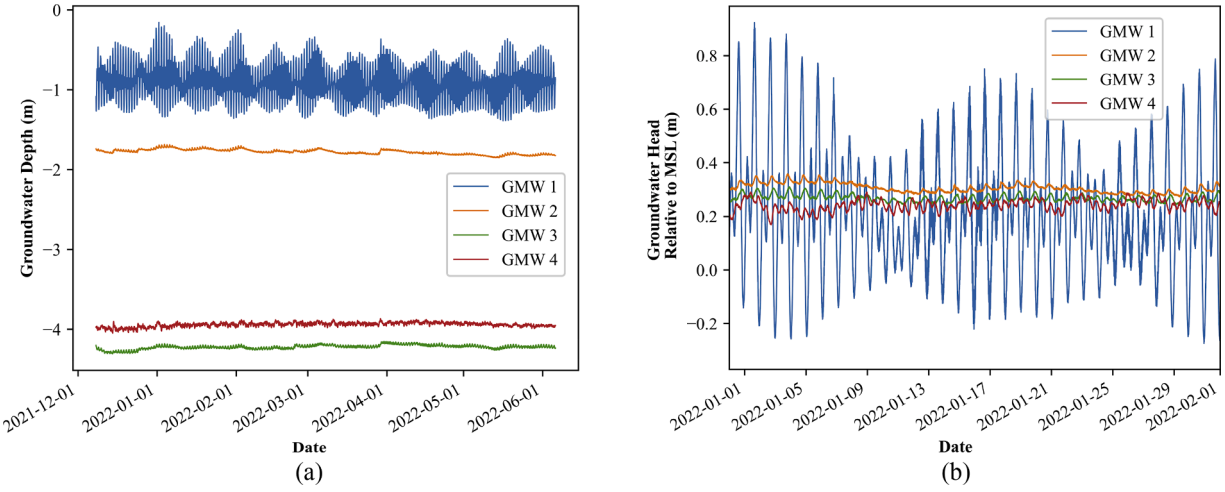

Fig. 10. Time series of (a) groundwater depth; and (b) groundwater head for the monitoring wells.

GWT fluctuations in the other wells across the city are less than 0.1 m, which is not impactful for urban infrastructure planning.

Tidal influence can be further quantified by the tidal efficiency (A), a measure of how damped the ocean tide amplitude is at a particular well, and the tidal phase lag (T_{lag}), a measure of the delay between the tidal forcing and GWT response. Table 7 shows a significant tidal influence at GMW 1 and relative damping at all other wells. From this table, the parameter A at GMW 1 is about 0.4, which is 1–2 orders of magnitude greater than that of GMW 2 − 4. In addition, $T_{lag} < 15$ min at GMW 1, while this parameter is more than 3 and 5 h at GMW 2 and 3, respectively. The tidal signal at GMW 4 is highly damped and distorted from the tidal forcing, and a phase lag cannot be determined because multiple plausible peaks in cross-correlation exist. From these possible peaks in cross-correlation, a range of tidal efficiency is reported for GMW 4 in Table 7. The high A and small T_{lag} values at GMW 1 are expected due to its proximity to the ocean and the relatively coarse sandy soil in the

Table 7
Tidal influence parameters in the monitoring groundwater wells.

Parameter	GMW 1	GMW 2	GMW 3	GMW 4
A (–)	0.393	0.007	0.008	0.004–0.007
T_{lag} (hr)	0.236	3.246	5.193	–

narrow area near the coastline. However, the tidal influences at GMW 2 and 3 are much smaller than our initial expectation considering their proximity to the Tijuana Estuary (30 m) and San Diego Bay (75 m), respectively. The significant damping of the tidal signal at these two wells near tidally-influenced water bodies suggests that the fine clay sediment underlying most of IB attenuates tidal fluctuations of GWT across the city [Web Soil Survey of The United States Department of Agriculture (2019)]. These findings are consistent with GWT observations from Honolulu, Hawaii, where significant damping of tidal influence was observed in a relict river channel composed of fine-grained sediment (Habel et al. 2017). Since GMW 4 in the center of IB is located on a similar soil type with a larger distance from the surrounding water bodies, a small tidal influence occurs.

Given the weak tidal variations in the groundwater observations, a steady-state GWT approximation is appropriate for the management and planning of the sewer infrastructure system. The soil type for IB is assumed to fall in the GMW 2–4 range. Thus, a steady-state groundwater model is developed for simulating spatial variations of GWT under different SLR scenarios. The modeled GWT at MSL is compared with temporal mean values of the observed GWT from the installed wells in Fig. 11. From this figure, there is a strong agreement between the modeled and observed data (0.02–0.06 m difference), which validates the applicability of the groundwater model in predicting the spatial distribution of GWT across IB.

3.2. Marine and subsurface flooding

The assessment of potential marine and subsurface inundations is the first step in understanding the sewer system's vulnerability to climate change. From Fig. 3 and Fig. 12, while Tijuana Estuary will be permanently impacted by marine inundation at higher SLR values, there will be minimal impacts on IB's urbanized area from this source of surface flooding. The presented results in Table 8 reveal that less than 2% of the populated region will be inundated at the high SLR scenario (i.e., a 2-m rise in the present-day sea level). It is worth noting that the areas near water bodies may be heavily impacted during temporary surface-water events. For example, the studies of Gallien (2016) and Merrifield et al. (2021) revealed that the IB's shoreline is notably vulnerable to dynamic wave-driven impacts. However, the dynamic conditions of the surrounding water bodies are not included in the present study due to their small effects on GWT and the sewer system's response across the city (discussed in the previous section).

Compared to marine inundation, subsurface flooding (i.e., groundwater emergence and shoaling) has a more widespread spatial extent including areas far from the coastline (Fig. 12 and Table 8 as the groundwater model outputs). Even in the current conditions, the GroundWater Depth (GWD) is less than 2 and 4 m in 5% and 24% of city areas, respectively. As a growing challenge for subterranean urban infrastructure systems, the SLR-driven groundwater lift will increase these numbers to 24% and 62% at SLR = 2 m. In addition, in the case of the extreme scenario of SLR = 3 m, almost the entire city (95% of the urbanized area) will experience a GWD < 6 m at the end of the century.

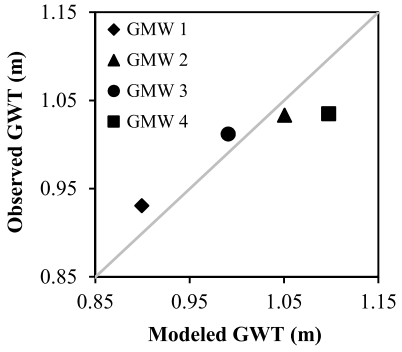

Fig. 11. Comparison of the modeled and observed values of groundwater table.

Having a general west-to-east direction, IB's sewer system is transmitting sewage flow away from the water bodies, and is not at risk of direct seawater intrusion (Fig. 4). However, due to the shallow GWT in IB, a substantial portion of the city's sewer pipelines may be at risk of GWI through their defects (adding a base flow to the system with a relatively steady rate). The presented results in Fig. 13 and Table 9 demonstrate that about 12% and 36% of the sewer pipeline lengths may be under GWT and susceptible to GWI at SLR = 0 and 2 m, respectively. A comparison of Fig. 12 and Fig. 13 reveals that the sewer pipelines below the GWT are typically located in low-lying regions of the city where the potential for a shallow GWT is the highest.

3.3. Defect flows in the sanitary sewer system

The calculation of defect flow magnitudes is initiated by WWI estimations. Once WWI is determined, the sewer infrastructure's response to GWI (adding a base flow to the system with a relatively steady rate) can be represented by deviations of dry-weather SSF from WWI. Then, differences between SSF in dry- and wet-weather conditions become the basis of RDII calculations (Fig. 7). The diurnal patterns of WWI also can be used for the estimation of daily peak values. According to Table 5, the modeled SSF values (from the calibrated model) agree well with the monitored data (from SFM 1–3) in both dry and wet weather conditions.

The water consumption in the study area during the monitoring period was approximately 8330 m^3/d based on the urban water use data from Pacific Institute (2018). According to Water Environment Federation (2010) and Mayer (2016), WWI is generally in the range of 70−75 percent of the supplied water (i.e., ranging from 5830 m^3/d to 6250 m^3/d for the study area). From Table 5, since the modeled WWI (with a total of 6079.5 m^3/d) perfectly fits in the expected range, the significant deviations of the monitored SSF from the modeled WWI can be attributed to defect flows (1330.5 and 2346.8 m^3/d respectively for dry- and wet-weather monitoring periods).

The estimations of GWI for different SLR scenarios are presented in Fig. 14. As expected, GWI increases with the rising sea level (red graph), and it grows about 4 times with 2 m of SLR (blue graph). In fact, the SLR-driven groundwater lift increases both A_{eff} and H_G parameters enlarging GWI [Eq. (3) and Fig. 9]. We assume that only defective conduits in the existing system (Fig. 5) are contributing to GWI in both current and future conditions. Nonetheless, higher GWI values are generally expected by extending structural damages to non-detective parts of the system over time. By considering the calibrated P values (section for the whole (2.3.4, system it was found that GWI can increase almost threefold in all SLR scenarios.

To improve the understanding of the extent of defect flows, Fig. 15 demonstrates the variations of SSF with SLR in both dry and wet-weather conditions. From Fig. 15(a), GWI increases hydraulic loads on the sewer system by 21% and 84% under current conditions and the high sea level scenario, SLR = 0 and 2 m, respectively. These numbers can be increased up to 49% and 120% during a 25-year rainfall event. The ratio of peak to mean SSF is presented in Fig. 15(b) for different oceanographic and meteorological conditions. In the current sea-level and dry-weather conditions, there might be a 33% uplift in SSF during peak hours. However, due to the higher contributions of GWI and RDII into SSF, this ratio may reduce almost to half in the high sea-level and wet-weather conditions.

Besides increasing the potential for Sanitary Sewer Overflow (SSO),

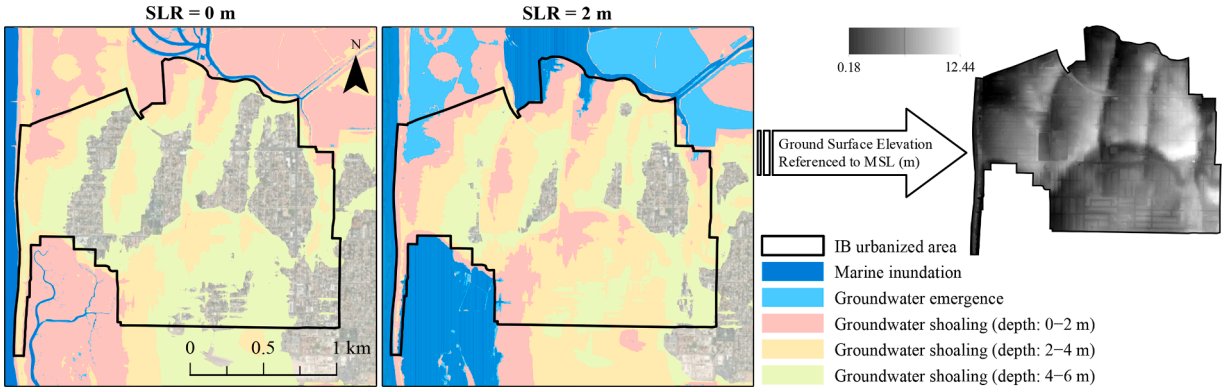

Fig. 12. Marine inundation and subsurface flooding in current and future conditions.

Table 8
Percentages of the IB urbanized area (total area = 5515,463 m^2) impacted by marine and subsurface flooding.

Source	SLR (m)			
	0	1	2	3
Marine inundation	0.0%	0.1%	1.8%	9.1%
Groundwater emergence	0.0%	0.2%	3.9%	9.8%
Groundwater shoaling with < 1 m depth	0.3%	4.2%	11.1%	20.2%
Groundwater shoaling with < 2 m depth	5.0%	11.7%	23.7%	36.0%
Groundwater shoaling with < 4 m depth	27.2%	41.9%	61.7%	75.3%
Groundwater shoaling with < 6 m depth	67.1%	80.7%	90.6%	94.7%

Table 9
Percentages of sewer pipes under groundwater table [= 100 × L_{eff} / (total length of 74,289 m)].

Range (m)	SLR (m)			
	0	1	2	3
$H_G > 5$	0.0%	0.0%	0.0%	0.1%
$H_G > 4$	0.0%	0.0%	0.2%	1.5%
$H_G > 3$	0.0%	0.2%	2.6%	7.4%
$H_G > 2$	0.2%	2.8%	9.4%	17.3%
$H_G > 1$	4.2%	11.6%	21.5%	34.4%
$H_G > 0$	12.3%	22.6%	35.8%	48.7%

which is known as an environmental catastrophe and discussed in the next section, the defect flows at least place a burden on wastewater collection systems and treatment facilities if all these elevated loads can be handled by the infrastructure. Based on our results, with 300 mm of total annual rainfall, the defect flows in IB's sewer system can be up to 0.5, 1.1, 1.9, and 2.7 million m^3/yr for SLR = 0, 1, 2, 3 m, respectively. In addition, unit costs related to the collection system and treatment plant are estimated at $0.61 and $0.81 per cubic meter of SSF [sewer service studies for The City of Imperial Beach (2021)]. Therefore, for SLR = 0, 1, 2, and 3 m scenarios, the defect flows may respectively cost the city an additional approximate amount of 0.7, 1.5, 2.7, and 3.9 million dollars each year (not to include their possible contributions in SSO and mitigation costs).

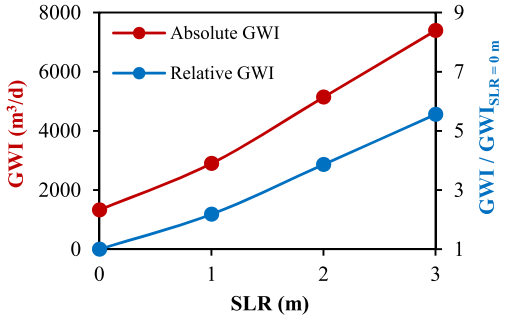

Fig. 14. Estimations of GroundWater Infiltration (GWI) into the sewer system.

3.4. Potential of sanitary sewer overflows

The potential for overflows in the sewer system is evaluated based on hydraulic conditions in its junctions (i.e., free, surcharged, or under-pressure flow). As shown in the legend of Fig. 16, in a free junction, water surface elevation [or Hydraulic Grade Line (HGL)] is lower than the crown of connecting conduits. However, a surcharged condition may occur by increasing SSF when connecting conduits get full of water. Due to further increases in SSF, sewer junctions eventually become

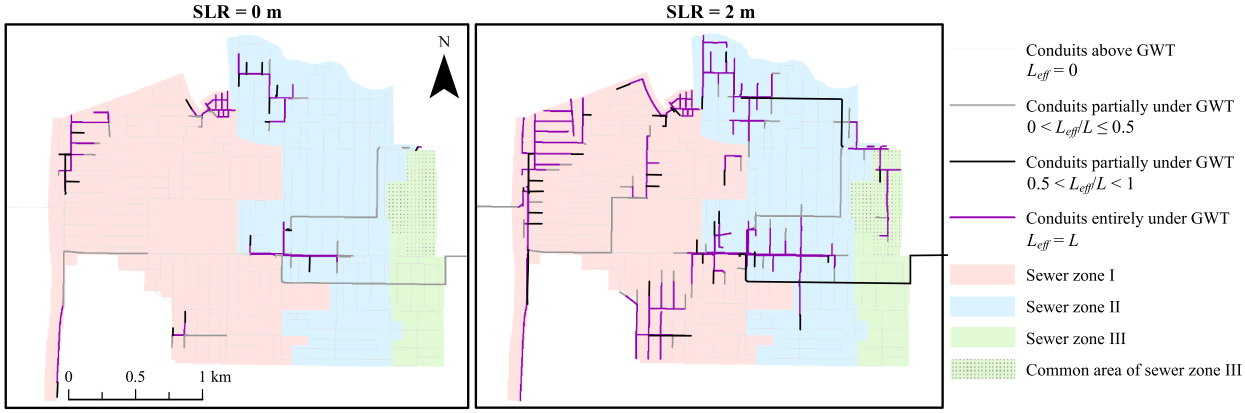

Fig. 13. Sewer pipelines under groundwater table in current and future sea levels.

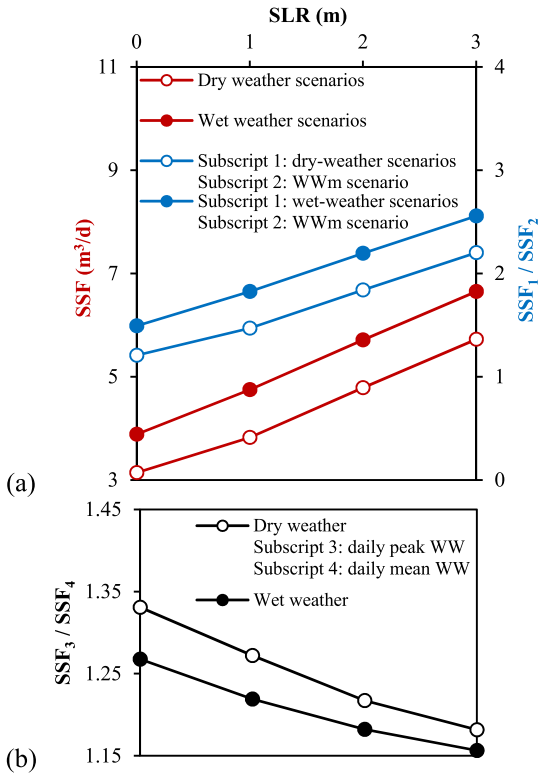

Fig. 15. Estimations of Sanitary Sewage Flow (SSF) by considering: (a) daily mean wastewater inflow; (b) daily peak wastewater inflow.

pressurized and vulnerable to SSO if Energy Grade Line (EGL = HGL + velocity head) exceeds the ground surface elevation.

The SSO potential of IB's sewer system is mapped in Fig. 16 for five scenarios in current and future conditions (defined in Table 6). As shown, even for the current sea-level conditions, there is some potential for SSO occurrences across the city, especially in the pressurized junctions. This point can be confirmed by 34 SSO events reported by the city since 2000 (internal reports of The City of IB shared with our team), which caused more than 74 m^3 of sewage spill in total. It is worth noting the real-world performance of the sewer system might be poorer in comparison to the presented results. For example, local blockages (e.g., debris, grease deposition, and root intrusion) in a sewer system can temporarily increase EGL in free or surcharged junctions and cause SSO.

From Fig. 16, SLR not only will shift the shoreline landward but also increase the SSO potential substantially through enlarging GWI contribution to SSF in a defective system. With 2 m of SLR, the number of pressurized junctions across the city is expected to increase from 13 to 22 and 30 in dry and wet-weather conditions, respectively. This number can be increased up to 73 during peak flow hours. With rising sea levels over the century, the area most impacted by SSO in the city will be kilometers away from the coastline (frequently impacted by dynamic sea-level events). In fact, the SSO hotspots will be more concentrated on the shallow-groundwater regions where the groundwater head over the defective sewer pipelines is the highest (depicted in Fig. 12 and Fig. 13). More challengingly, SSO events can be considerably more widespread and severe due to larger amounts of WWI and RDII during peak flow hours and wet-weather periods, respectively (leading to further increases in the hydraulic loadings on the system). These findings confirm the importance of considering the compound impacts of coastal stressors on urban infrastructure systems.

Based on the CCTV assessment of defective conduits and the results obtained from the present study, a holistic approach is presented and implemented for prioritizing sewer system repairs (Fig. 17). As a comprehensive index, Sanitary Sewer Vulnerability Index (SSVI) involves different structural, hydrological, and hydraulic conditions in the

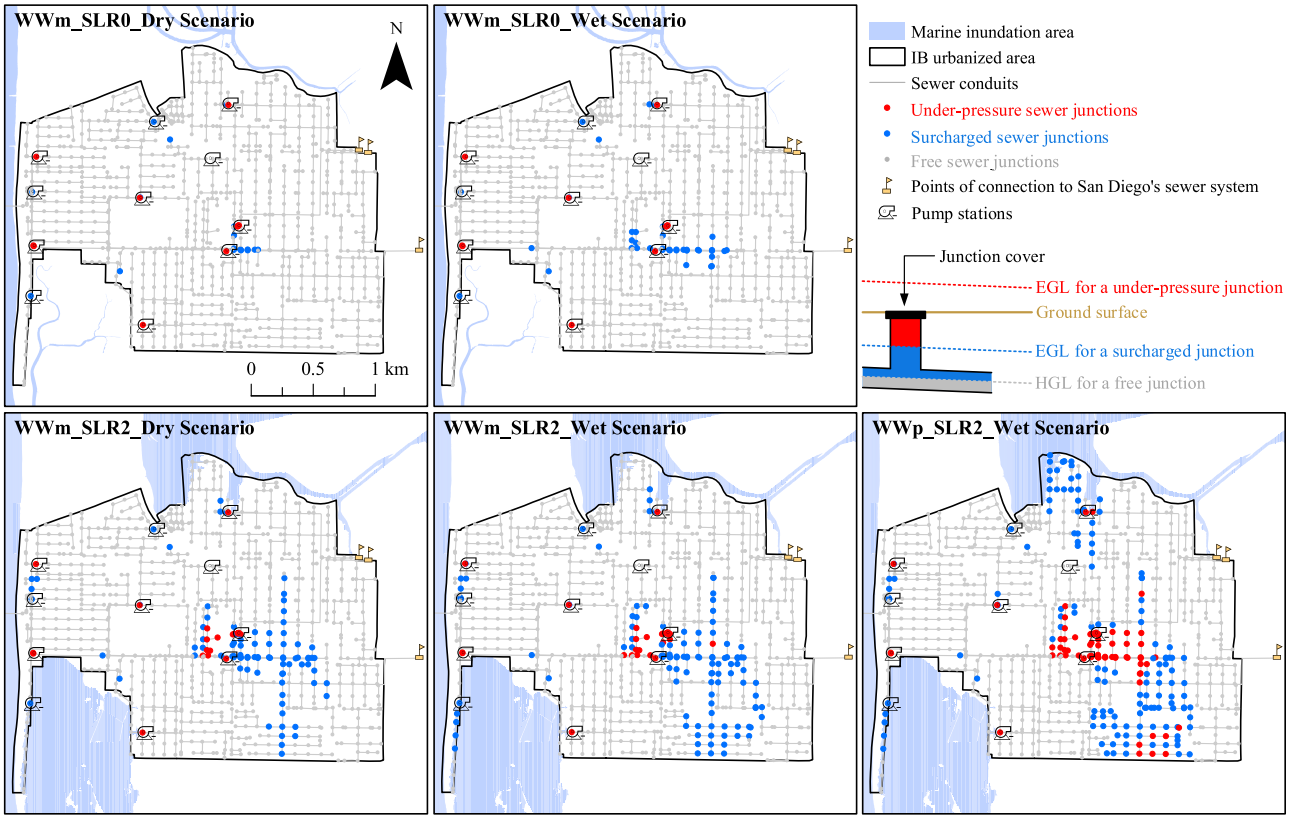

Fig. 16. Mapping of SSO potential for five selected scenarios (defined in Table 6).

rehabilitation priority plan. From Fig. 17, each defective conduit is given a structural damage degree of slight, moderate, or high. In addition, higher degrees of vulnerability are assigned to defective conduits immersed in groundwater at lower values of SLR (which are more prone to GWI and additional structural deterioration). The SSVI values for defective conduits are also rated based on their proximity to junctions with higher hydraulic head or SSO potential. As a result, each defective conduit in IB's sewer system is given a low, moderate, high, or urgent priority, which demands the most immediate action for rehabilitation. It is worth noting that the rehabilitation priority plan will need to be updated to account for further structural damages over the century.

From the rehabilitation priority map shown in Fig. 17(c), the higher priority repairs (SSVI $\geq$ 5) are mostly located in the low-lying areas (Fig. 12), which are more susceptible to experiencing defect flows (Fig. 13) and SSO events (Fig. 16). In addition, while The City of IB is currently paying most attention to the coast in its SLR planning projects, Fig. 17(c) reveals that the urgent-priority rehabilitation of the water infrastructure is mostly needed further inland (~2 km from the coastline). This point emphasizes the importance of considering the interactions of oceanographic, hydrological, and meteorological processes in the planning of urban infrastructure systems and developing efficient adaptation strategies against climate change and SLR.

To improve the understanding of emerging climate change impacts, future studies are needed on the following topics:

- A major point for mitigation plans is the site-specificity of coastal climate change impacts on the urban infrastructure. This is due to the variety of urban infrastructure settings in different areas. For instance, communities with similar SLR challenges may have different types of combined or separate sewer networks. The geography, geology, and meteorology of communities also add many other important factors, which can't be neglected for arriving at scientific outcomes. As a result, a new 5-year project has been launched (Davani 2023) to study a set of US West-Coast communities in high detail.
- Recent field-based studies demonstrate that wastewater exfiltration from defective sewer pipes is a source of coastal aquifer pollution (McKenzie et al. 2021; Nguyen et al. 2021). While wastewater exfiltration processes are beyond the scope of this research, they should be considered in modeling procedures and comprehensive rehabilitation strategies.
- Considering the useful life expiration of sewer pipelines by 2100 and the rapid development of sensing and communication technologies using Artificial Intelligence (AI) applications, a significant shift from reactive to real-time and smart monitoring of urban water infrastructure systems will be required for addressing climate change

Index	Degree of sewer structural damages			Sewer inundation by groundwater at different greenhouse-gas emission scenarios				Flow condition in downstream junction		
	Slight	Moderate	Severe	Low (SLR = 0 m)	Moderate (SLR = 1 m)	High (SLR = 2 m)	Extreme (SLR = 3 m)	Free	Surcharged	Pressurized
Sanitary sewer deficiency index (A)	2	4	8							
Groundwater head index (B)				8	4	2	1			
SSO potential index (C)								2	4	8

(a)

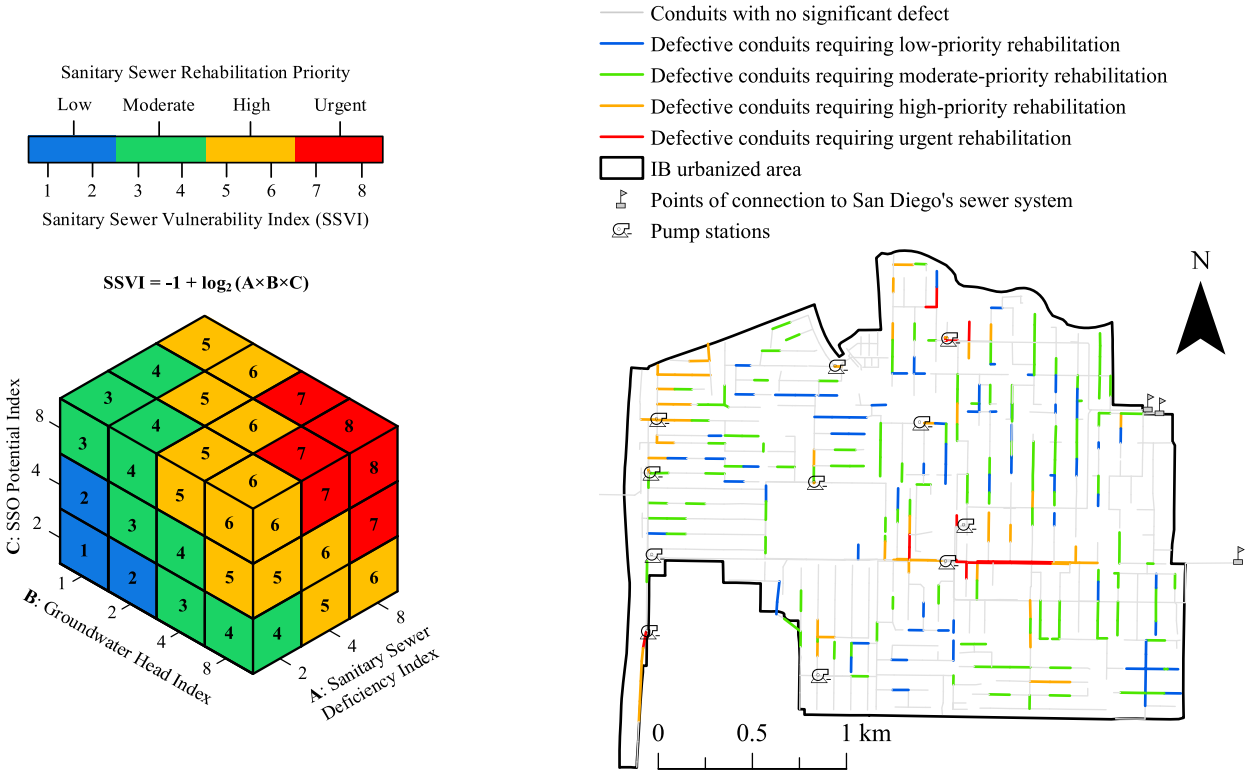

(b) (c)

Fig. 17. Rehabilitation priority plan: (a) definition of involved indices; (b) visualization of vulnerability matrix; (c) Implementation on IB's sewer system.

issues. By leveraging state-of-the-art computer vision techniques, preliminary studies in the literature [such as Tan et al. (2021) and Oh et al. (2022)] have provided promising prospects for implementing AI-based models for sewer defect detection from massive CCTV videos.

4. Conclusions

This paper studies compound impacts of climate change (i.e., SLR- and rainfall-driven groundwater infiltration and inflow) on the sanitary sewer system in a coastal city in Southern California [Imperial Beach (IB)]. The results lead to the following conclusions:

- Weak tidal amplitudes (< 0.1 m) in GWT observations support the development of a steady-state groundwater model. For SLR $= 2$ m, less than 2% of the city will be below sea level (neglecting wave contributions). However, GWD will be less than 2 m in $\sim 1/4$ of the city area. In these circumstances, more than 1/3 of sewer pipelines might be immersed in groundwater (susceptible to GWI).
- Besides a landward shift in the shoreline, SLR also can impact the sewer performance kilometers away from water bodies. With the current sea level, defect flows (i.e., GWI and RDII) increase hydraulic loads on the system by 21% and 49% in dry- and wet-weather conditions, respectively. With 2-m SLR, GWI grows approximately 4 times: defect flows increase hydraulic loads by 84% and 120% in dry- and wet-weather conditions, respectively. The additional sewage will cost the city approximately $3 M each year.
- Defect flows also increase the potential of SSO. With a 2 m SLR, there will be about 70% and 130% growths in the number of pressurized sewer junctions across the city in dry- and wet-weather conditions, respectively. The number can increase up to 2.3 times during peak flow hours. For SLR planning projects, the city is currently paying the most attention to the coast. However, by considering the interactions of oceanographic, hydrological, and meteorological processes, the proposed vulnerability index gives the highest rehabilitation priority to some parts of wastewater infrastructure in the middle of the city.
- A major source of uncertainty in the present study is the aquifer's geotechnical characteristics (e.g. aquifer inhomogeneity and anisotropy). Due to the lack of data, a sensitivity analysis was employed for the approximation of **K** (Sangsefidi et al. 2023). However, geospatial variations of **K** across the city still remain a source of uncertainty in the presented results. Typically, the narrow sandy layers near the coastline result in higher conductivity compared to inland clay layers. Therefore, this uncertainty is expected to cause an underestimation of defect flows toward the western regions of our case study.

CRediT authorship contribution statement

Yousef Sangsefidi: Conceptualization, Methodology, Software, Validation, Formal analysis, Investigation. **Austin Barnes:** Data curation, Writing – original draft, Writing – review & editing, Visualization, Methodology, Investigation, Data curation, Writing – review & editing, Visualization. **Mark Merrifield:** Methodology, Resources, Writing – review & editing, Project administration, Funding acquisition. **Hassan Davani:** Conceptualization, Methodology, Resources, Writing – review & editing, Supervision, Project administration, Funding acquisition.

Declaration of Competing Interest

The authors declare that they have no known competing financial interests or personal relationships that could have appeared to influence the work reported in this paper.

Data availability

Data will be made available on request.

Acknowledgments

This research has been supported by the National Science Foundation under Grants No. 2113987, 2113984, and 2239602. Additionally, this publication has been produced with support from the National Sea Grant College Program, National Oceanic and Atmospheric Administration, U.S. Department of Commerce, under grant number A22OAR4170104. We appreciate the support of Computational Hydraulics Int. (CHI), Waterloo Hydrogeologic, and The City of Imperial Beach (particularly Mr. Chris Helmer) for providing us with access to the PCSWMM license, Visual MODFLOW Flex license, and sewer system characteristics as well as sewage flow measurements, respectively.

References

Arkema, K. K., Guannel, G., Verutes, G., Wood, S. A., Guerry, A., Ruckelshaus, M., Kareiva, P., Lacayo, M., & Silver, J. M. (2013). Coastal habitats shield people and property from sea-level rise and storms. *Nature Climate Change, 3*(10), 913–918.

Badaruddin, S., Werner, A. D., & Morgan, L. K. (2015). Water table salinization due to seawater intrusion. *Water Resources Research, 51*(10), 8397–8408.

Befus, K. M., Barnard, P. L., Hoover, D. J., Finzi Hart, J. A., & Voss, C. I (2020). Increasing threat of coastal groundwater hazards from sea-level rise in California. *Nature Climate Change, 10*(10), 946–952.

Bevacqua, E., Maraun, D., Vousdoukas, M. I., Voukouvalas, E., Vrac, M., Mentaschi, L., & Widmann, M. (2019). Higher probability of compound flooding from precipitation and storm surge in Europe under anthropogenic climate change. *Science Advances, 5*(9), eaaw5531.

City of San Diego (2015). "Sewer design guide".

Cooper, H. M., Zhang, C., & Selch, D (2015). Incorporating uncertainty of groundwater modeling in sea-level rise assessment: A case study in South Florida. *Climatic Change, 129*(1), 281–294.

Davani, H. (2023). Environmental sustainability of combined versus separate sewer systems along the U.S. West Coast. *National Science Foundation* (Award Number: 2239602).

Dirckx, G., Van Daele, S., & Hellinck, N. (2016). Groundwater Infiltration Potential (GWIP) as an aid to determining the cause of dilution of waste water. *Journal of Hydrology, 542*, 474–486.

Domínguez-Vázquez, D., Jacobs, G. B., & Tartakovsky, D. M. (2021). Lagrangian models of particle-laden flows with stochastic forcing: Monte Carlo, moment equations, and method of distributions analyses. *Physics of Fluids, 33*, Article 033326.

Domínguez-Vázquez, D., Klose, B. F., & Jacobs, G. B. (2023). Closed SPARSE—A predictive particle cloud tracer. *International Journal of Multiphase Flow, 161*, 104375.

Engineering ToolBox (2004a). "Fluid flow friction loss - Hazen-Williams coefficients." <https://tinyurl.com/6uamkz7b>. (October 1, 2022).

Engineering ToolBox (2004b). "Manning's roughness coefficients." <https://tinyurl.com/56dwket5>. (October 1, 2022).

Fischer, E. M., Sedláček, J., Hawkins, E., & Knutti, R. (2014). Models agree on forced response pattern of precipitation and temperature extremes. *Geophysical Research Letters, 41*(23), 8554–8562.

Frost, W. H. (2006). Minor loss coefficients for storm drain modeling with SWMM. *Journal of Water Management Modeling*, 517–546. R225-23.

Fung, A., & Babcock, R. (2020). A flow-calibrated method to project groundwater infiltration into coastal sewers affected by sea level rise. *Water, 12*(7).

Gallien, T. W. (2016). Validated coastal flood modeling at Imperial Beach, California: Comparing total water level, empirical and numerical overtopping methodologies. *Coastal Engineering, 111*, 95–104.

Gold, A. C., Brown, C. M., Thompson, S. P., & Piehler, M. F. (2022). Inundation of stormwater infrastructure is common and increases risk of flooding in coastal urban areas along the US Atlantic Coast. *Earth's Future, 10*(3), Article e2021EF002139.

Guo, S., & Zhu, D. Z. (2017). Soil and groundwater erosion rates into a sewer pipe crack. *Journal of Hydraulic Engineering, 143*(7), Article 06017008.

Habel, S., Fletcher, C. H., Anderson, T. R., & Thompson, P. R. (2020). Sea-level rise induced multi-mechanism flooding and contribution to urban infrastructure failure. *Scientific reports, 10*(1), 3796-3796.

Habel, S., Fletcher, C. H., Rotzoll, K., & El-Kadi, A. I. (2017). Development of a model to simulate groundwater inundation induced by sea-level rise and high tides in Honolulu, Hawaii. *Water Research, 114*, 122–134.

Harbaugh, A. W. (2005). *MODFLOW-2005 : The U.S. geological survey modular groundwater model—the ground-water flow process*. USGS, USA: Techniques and Methods.

Kirezci, E., Young, I. R., Ranasinghe, R., Muis, S., Nicholls, R. J., Lincke, D., & Hinkel, J. (2020). Projections of global-scale extreme sea levels and resulting episodic coastal flooding over the 21st Century. *Scientific Reports, 10*(1), 11629.

Kopp, R. E., Kemp, A. C., Bittermann, K., Horton, B. P., Donnelly, J. P., Gehrels, W. R., Hay, C. C., Mitrovica, J. X., Morrow, E. D., & Rahmstorf, S. (2016). Temperature-

driven global sea-level variability in the Common Era. *Proceedings of the National Academy of Sciences, 113*(11), E1434–E1441.
Laster Grip, I., Haghighatafshar, S., & Aspegren, H (2021). A methodology for the assessment of compound sea level and rainfall impact on urban drainage networks in a coastal city under climate change. *City and Environment Interactions, 12*, Article 100074.
Liu, T., Ramirez-Marquez, J. E., Jagupilla, S. C., & Prigiobbe, V. (2021). Combining a statistical model with machine learning to predict groundwater flooding (or infiltration) into sewer networks. *Journal of Hydrology, 603*, Article 126916.
Liu, T., Su, X., & Prigiobbe, V. (2018). *Groundwater-Sewer interaction in urban coastal areas*. Water.
Lu, C., Chen, Y., Zhang, C., & Luo, J. (2013). Steady-state freshwater–seawater mixing zone in stratified coastal aquifers. *Journal of Hydrology, 505*, 24–34.
Masson-Delmotte, V., Zhai, P., Pirani, A., Connors, S. L., Péan, C., Berger, S., Caud, N., Chen, Y., Goldfarb, L., & Gomis, M. (2021). Climate change 2021: The physical science basis. In *Proceedings of the Contribution of working group I to the sixth assessment report of the intergovernmental panel on climate change* (p. 2).
Mayer, P. W. (2016). Water research foundation study documents water conservation potential and more efficiency in households. *Journal AWWA, 108*(10), 31–40.
McKenzie, T., Habel, S., & Dulai, H. (2021). Sea-level rise drives wastewater leakage to coastal waters and storm drains. *Limnology and Oceanography Letters, 6*(3), 154–163.
Mehdizadeh, S. S., Werner, A. D., Vafaie, F., & Badaruddin, S. (2014). Vertical leakage in sharp-interface seawater intrusion models of layered coastal aquifers. *Journal of Hydrology, 519*, 1097–1107.
Merrifield, M. A., Johnson, M., Guza, R. T., Fiedler, J. W., Young, A. P., Henderson, C. S., Lange, A. M. Z., O'Reilly, W. C., Ludka, B. C., Okihiro, M., Gallien, T., Pappas, K., Engeman, L., Behrens, J., & Terrill, E (2021). An early warning system for wave-driven coastal flooding at Imperial Beach, CA. *Natural Hazards, 108*(3), 2591–2612.
Nguyen, H. H., Peche, A., & Venohr, M. (2021). Modelling of sewer exfiltration to groundwater in urban wastewater systems: a critical review. *Journal of Hydrology, 596*, Article 126130.
Oh, C., Dang, L. M., Han, D., & Moon, H. (2022). Robust sewer defect detection with text analysis based on deep learning. *IEEE access : practical innovations, open solutions, 10*, 46224–46237.
Pacific Institute (2018). "Urban water use data." <www.pacinst.org>. (October 1, 2022).
Plane, E., Hill, K., & May, C (2019). *A rapid assessment method to identify potential groundwater flooding hotspots as sea levels rise in coastal cities*. Water.
Reitz, M., Sanford, W. E., Senay, G. B., & Cazenas, J. (2017). Annual estimates of recharge, quick-flow runoff, and evapotranspiration for the contiguous US using empirical regression equations. *JAWRA Journal of the American Water Resources Association, 53*(4), 961–983.
Rezaee, M., & Tabesh, M. (2022). Effects of inflow, infiltration, and exfiltration on water footprint increase of a sewer system: A case study of Tehran. *Sustainable Cities and Society, 79*, Article 103707.
Rossi, R. J., & Toran, L. (2019). Exploring the potential for groundwater inundation in coastal US cities due to interactions between sewer infrastructure and global change. *Environmental Earth Sciences, 78*(8), 258.
Rossman, L.A. (2015). "Storm water management model user's manual version 5.1".
Rotzoll, K., & Fletcher, C. H. (2013). Assessment of groundwater inundation as a consequence of sea-level rise. *Nature Climate Change, 3*(5), 477–481.
Sangsefidi, Y., Bagheri, K., Davani, H., & Merrifield, M. (2023). Data analysis and integrated modeling of compound flooding impacts on coastal drainage infrastructure under a changing climate. *Journal of Hydrology, 616*, Article 128823.
Stuart, S. L. (2008). *Groundwater and surface water interactions at the Tijuana Estuary, San Diego, California*. MS Thesis. USA: San Diego State University.
Su, X., Belvedere, P., Tosco, T., & Prigiobbe, V. (2022). "Studying the effect of sea level rise on nuisance flooding due to groundwater in a coastal urban area with aging infrastructure. *Urban Climate, 43*, Article 101164.
Swamee, P. K., & Swamee, N. (2010). Discharge equation of a circular sharp-crested orifice. *Journal of Hydraulic Research, 48*(1), 106–107.
Sweet, W. V., Hamlington, B. D., Kopp, R. E., Weaver, C. P., Barnard, P. L., Bekaert, D., Brooks, W., Craghan, M., Dusek, G., Frederikse, T., Garner, G., Genz, A. S., Krasting, J. P., Larour, E., Marcy, D., Marra, J. J., Obeysekera, J., Osler, M., Pendleton, M., Roman, D., Schmied, L., Veatch, W., White, K. D., & Zuzak, C. (2022). *Global and Regional Sea Level Rise Scenarios for the United States: Updated Mean Projections and Extreme Water Level Probabilities Along U.S. Coastlines*. National Oceanic and Atmospheric Administration, National Ocean Service, Silver Spring. NOAA Technical Report NOS 01.
Tan, Y., Cai, R., Li, J., Chen, P., & Wang, M (2021). Automatic detection of sewer defects based on improved you only look once algorithm. *Automation in Construction, 131*, Article 103912.
Tavakol-Davani, H., Goharian, E., Hansen, C. H., Tavakol-Davani, H., Apul, D., & Burian, S. J. (2016). How does climate change affect combined sewer overflow in a system benefiting from rainwater harvesting systems? *Sustainable Cities and Society, 27*, 430–438.
Teimoori, S., O'Leary, B. F., & Miller, C. J. (2021). *Modeling shallow urban groundwater at regional and local scales: A case study in detroit, mi, 13* p. 1515). Water.
The City of Imperial Beach (2021). "Sewer service charge and capacity fee study".
Thompson, P. R., Widlansky, M. J., Hamlington, B. D., Merrifield, M. A., Marra, J. J., Mitchum, G. T., & Sweet, W. (2021). Rapid increases and extreme months in projections of United States high-tide flooding. *Nature Climate Change, 11*(7), 584–590.
Trenberth, K. E. (2011). Changes in precipitation with climate change. *Climate Research, 47*, 123–138.
United States Department of Agriculture (2019). "Web soil survey." <http://websoilsurvey.sc.egov.usda.gov/>. (October 1, 2022).
Vitousek, S., Barnard, P. L., Fletcher, C. H., Frazer, N., Erikson, L., & Storlazzi, C. D. (2017). Doubling of coastal flooding frequency within decades due to sea-level rise. *Scientific Reports, 7*(1), 1399.
Water Environment Federation (2010). Design of municipal wastewater treatment plants: Wef manual of practice no. 8, McGraw-Hill Education, New York.
Waterloo Hydrogeologic (2021). "Visual modflow flex 7.0 integrated conceptual & numerical groundwater modeling software." Waterloo, ON, Canada.
Watson, T. A., Werner, A. D., & Simmons, C. T. (2010). Transience of seawater intrusion in response to sea level rise. *Water Resources Research, 46*(12).
Zhao, Z., Yin, H., Xu, Z., Peng, J., & Yu, Z (2020). Pin-pointing groundwater infiltration into urban sewers using chemical tracer in conjunction with physically based optimization model. *Water Research, 175*, Article 115689.